SLAC-PUB-14056

Energy gaps in the failed high-T_c superconductor $La_{1.875}Ba_{0.125}CuO_4$

Rui-Hua He[1], Kiyohisa Tanaka[1,2,6], Sung-Kwan Mo[1,2], Takao Sasagawa[1,4], Masaki Fujita[3], Tadashi Adachi[5], Norman Mannella[1,2*], Kazuyoshi Yamada[3], Yoji Koike[5], Zahid Hussain[2], Zhi-Xun Shen[1]

[1]*Department of Physics, Applied Physics and Stanford Synchrotron Radiation Laboratory, Stanford University, Stanford, California 94305, USA*

[2]*Advanced Light Source, Lawrence Berkeley National Lab, Berkeley, California 94720, USA*

[3]*Institute of Materials Research, Tohoku University, Sendai 980-8577, Japan*

[4]*Materials and Structures Laboratory, Tokyo Institute of Technology, Kanagawa 226-8503, Japan*

[5]*Department of Applied Physics, Tohoku University, Sendai 980-8579, Japan and*

[6]*Department of Physics, Osaka University, Osaka 560-0043, Japan*

(Dated: February 14, 2008)

* Present address: Department of Physics and Astronomy, University of Tennessee, Knoxville, Tennessee 37996, USA

Work supported in part by US Department of Energy contract DE-AC02-76SF00515.

A central issue on high-T_c superconductivity is the nature of the normal-state gap (pseudogap) [1] in the underdoped regime and its relationship with superconductivity. Despite persistent efforts, theoretical ideas for the pseudogap evolve around fluctuating superconductivity [2], competing order [3, 4, 5, 6, 7, 8] and spectral weight suppression due to many-body effects [9]. Recently, while some experiments in the superconducting state indicate a distinction between the superconducting gap and pseudogap [10, 11, 12, 13, 14], others in the normal state, either by extrapolation from high-temperature data [15] or directly from $La_{1.875}Ba_{0.125}CuO_4$ (LBCO-1/8) at low temperature [16], suggest the ground-state pseudogap is a single gap of d-wave [17] form. Here we report angle-resolved photoemission (ARPES) data from LBCO-1/8, collected with improved experimental conditions, that reveal the ground-state pseudogap has a pronounced deviation from the simple d-wave form. It contains two distinct components: a d-wave component within an extended region around the node and the other abruptly enhanced close to the antinode, pointing to a dual nature of the pseudogap in this failed high-T_c superconductor which involves a possible precursor pairing energy scale around the node and another of different but unknown origin near the antinode.

The first high-T_c superconductor discovered, $La_{2-x}Ba_xCuO_4$ (LBCO), holds a unique position in the field because of an anomalously strong bulk T_c suppression near $x = 1/8$. Right around this "magic" doping level, scattering experiments by neutron [18, 19] and X-ray [20] find a static spin and charge (stripe) order. By itself, this observation raises a series of intriguing questions: whether the stripe order is a competing order that suppresses the superconductivity in LBCO-1/8 and, if the answer is positive, which aspect, the pairing strength or the phase coherence, is involved in the T_c suppression and how this mechanism applies to other dopings or families. For our investigation of the "ground-state" pseudogap, as defined in Ref. [16] that ignores the residual superconductivity, its sufficiently high doping yet extremely low bulk T_c (~ 4 K) makes LBCO-1/8 an ideal system: especially for the small-gap measurement near the node, difficulties due to either the unscreened disorder potential, a problem for extremely low doping, or trivial thermal broadening, a problem above T_c for higher doping, are circumvented.

While thermal effects require an extrapolation from high-temperature data to obtain the ground state physics [15], a direct measurement on LBCO-1/8 at low temperature has been made [16]. With experimental resolutions compromised to obtain sufficient signal to noise, a simple *d*-wave gap function is reported with no discernible nodal quasi-particles found. Given the importance of this issue, we have performed an ARPES [21] study of LBCO-1/8 at $T>T_c$ with much improved resolutions in a measurement geometry favorable for the detection of nodal quasi-particles (see Fig. 1 & Supplementary Section I). Our data provide two important new insights. First, there is a well-defined nodal quasi-particle peak suggesting nodal quasi-particles can exist in the stripe ordered state. Second, there is a rich gap structure suggesting the pseudogap physics is more elaborate than the simple *d*-wave version. In particular, a new kind of pseudogap, which is not smoothly connected to the usual one tied to the antinodal region, can exist in the nodal region when superconductivity is suppressed due to the loss of phase coherence.

As shown in Fig. 1, there exists a well-defined quasi-particle peak in the energy distribution curves (EDC's) at the Fermi crossing points (k_F's) around the node. Upon dispersion towards the antinode, the lineshape quickly becomes incoherent. Data taken with different photon energies ($h\nu$'s) in different Brillouin zones (BZ's) show consistent results (Supplementary Fig. S1), providing the first unambiguous piece of direct evidence that nodal quasi-particles survive in the stripe ordered state. This suggests these two seemingly very different aspects of cuprate phenomenology can be compatible with each other [22].

The observation of quasi-particle peaks in the EDC's gives a firm foundation for the gap analysis around the node. However, given the small gap size as well as a relatively small peak-background intensity ratio and large quasi-particle peak linewidth (Γ) (Fig. 1d), quantitative determination of the gap is non-trivial in LBCO-1/8. In the following, we will present analysis that addresses two important aspects of our data: i) the gap measured by the leading edge gap (LEG) method, same as employed by Ref. [16], is shown to have two components and cannot fit a simple *d*-wave form (Figs. 2 & 4); ii) the gap around the node, measured either by the LEG method (Fig. 2) or by a curve fitting procedure commonly used in the field (Fig. 3), is shown to be *d*-wave like with a finite gap slope.

In Fig. 2a, from the systematic shift of the leading-edge midpoint along the energy axis, we notice the LEG keeps increasing from the node towards the antinode with the rate

of increase getting larger close to the antinode. This is more clearly shown in Fig. 2b where the momentum dependence of the extracted LEG from two selected samples is plotted. Consistent results are obtained at different times after sample cleaving, showing no signs of sample aging which could affect small-gap measurements, and in different BZ's with different hν's on another sample. They unanimously point to a pronounced deviation of the gap function from the simple d-wave form. As detailed in Supplementary Section IIIB, C& IV, this observation goes beyond the interpretation based on either a simple d-wave gap under the influence of experimental resolutions (Supplementary Fig. S10) and the lineshape decoherence towards the antinode (Supplementary Fig. S11) or a single pairing gap with the inclusion of higher d-wave gap harmonics [23] (Supplementary Fig. S7). It naturally reveals a striking characteristic: this normal-state gap has two distinct components, with the one around the node (the nodal gap) exhibiting a simple d-wave form, i.e., a linear dependence with respect to (w.r.t.) $[cos(k_x) - cos(k_y)]/2$, along the underlying FS over a significant momentum range and the other setting in near the antinode (the antinodal gap) which deviates sharply from its nodal counterpart.

Although it is clear that the LEG opens in a d-wave fashion around the node (inset of Fig. 2a), it is too crude to conclude the real gap (Δ) function of the system is also simple d-wave like because the leading edge shift in principle can be due to the variation in Γ even if Δ is fixed [24]. This alternative has to be explored especially for LBCO-1/8 where $\Gamma >> \Delta$ near the node. Thus, we fit the E_F-symmetrized EDC's at k_F to a phenomenological model [25] which assumes a self energy, $\Sigma(k_F, \omega) = -i\Gamma + \frac{\Delta^2}{\omega}$ (Fit Model), where Γ and Δ are subject to the fit (Fig. 3a). Because of the small peak-background ratio, the fitting results are somewhat affected by the background subtraction. In Fig. 3b, we show the results of Δ without any background subtraction, or with an MDC constant background or an EDC integral background subtraction (Supplementary Fig. S5). Two general trends of the results are: i) regardless of methods for background subtraction, an initial gap slope is robustly defined close to the node where quasi-particle peaks are clearly present in e1 $\sim$ e3; ii) upon weakening of the peak feature, a large background dependence appears starting from e4. For e4, with more background subtracted from the high binding energy side of the peak feature, Δ decreases and tends to fall onto the initial gap slope. For the completeness of our analysis, we have also shown in Supplementary Fig. S6 fitting results based on another model that fits the data less well.

While the quantitative gap values are model dependent, its d-wave form remains robust (Supplementary Section IID).

Summarizing the above, both the model independent (the LEG method) and model dependent (the curve fitting procedure) gap analysis suggest that the nodal gap opens in a d-wave fashion with a finite slope. Despite its presence in the normal state, it is highly suggestive that this nodal gap is of a pairing origin based on the following reasons: i) its d-wave form is consistent of the generic pairing symmetry of cuprate superconductors, particularly in La-based cuprates, where a similar gap in the nodal region is found to be related to superconductivity [12]; ii) its gap slope strikingly coincides within error bars with those of $La_{2-x}Sr_xCuO_4$ (LSCO) $x = 0.11$ [29] and LBCO $x = 0.083$ [30] (T_c=26 K and 23 K, respectively, see Supplementary Fig. S8 for raw data), which are both in the superconducting state (Fig. 4a). Compared with the one analyzed using Fit Model in Bi2212 of a similar doping level (UD75K in Ref. [11]) at low temperature, it exhibits a factor of ~ 2 reduction, reminiscent of the optimal T_c difference of these two families; iii) its susceptibility to thermal smearing in contrast to its antinodal counterpart (Fig. 4b) is reminiscent of the cases in other superconducting cuprates [11, 12]. The existence of precursor pairing in the normal state of LBCO-1/8 is further supported by recent transport measurements [26]. A drop in the in-plane resistivity at $T_{2D} \sim 40$ K, where the concurrent stripe (as a density wave) formation would often result in an increase of resistivity, implies an onset of superconducting fluctuations. Although the coincidence of its partial closing with the simultaneous resistivity increase at $T=T_{2D}$ upon heating (Fig. 4b) suggests the precursor pairing origin of the nodal gap rather than the conventional density wave type, understanding the relationship between these two coexisting orders in the system at $T<T_{2D}$ still poses a challenge.

On the other hand, the pairing strength, as reflected by the slope of the nodal pairing gap, is comparable in LBCO-1/8 and its neighboring compounds of much higher bulk T_c values (Fig. 4a). Hence, a natural explanation for the bulk T_c suppression in LBCO-1/8 is its lack of a global superconducting phase coherence. Interestingly, this loss of superconducting phase coherence coincides with the stabilization of the stripe order at $x\sim1/8$. Intrigued by this, theorists have proposed that the global superconducting phase coherence can be prohibited via the dynamical interlayer decoupling in the system where superconductivity is modulated by the stripe order of some specific configurations [27, 28].

Nevertheless, the modulated superconductivity of a non-zero wave vector generally does not produce a d-wave gap with a point node as observed here. Our finding would put a strong constraint on future theoretical attempts to resolve the microscopic mechanism for the failure of high-T_c superconductivity in LBCO-1/8.

As suggested by its different momentum dependence from its nodal counterpart, the antinodal pseudogap may have a different origin, which has been the subject for intense discussions in literature [2, 3, 4, 5, 6, 7, 8, 9]. Generally, as inferred from Supplementary Fig. S11, a similar antinodal phenomenology as we observed can be achieved either by i) a true gap opening together with a strong quasi-particle scattering (the $\Delta - \Gamma$ physics) or by ii) a great suppression of the quasi-particle spectral weight (the Z physics). While attempts of Scheme i) working in the weak coupling approach can produce a qualitatively similar quasi-particle gap structure by considering the competition between superconductivity and the charge [6, 7] or/and spin [8, 27] density wave order, Scheme ii) demands a strong-coupling route (e.g., Ref. [9]) where the extended quasi-particle analysis as presented above might break down due to its incapability of capturing the lowest-lying excitations of a vanishing spectral weight. In any case, new physics other than the nodal-type precursor pairing alone is required to fully capture the essence of the antinodal pseudogap.

In contrast to the notion of a simple d-wave nodal liquid as the pseudogap ground state which is directly derived from the antinodal pseudogap [15, 16], our observation of an apparent break-up of the gap function suggests a very different picture. It reveals a much richer pseudogap physics with its two aspects manifesting differently in distinct momentum regions, i.e., the nodal precursor pairing and the antinodal pseudogap of different but unknown origin. These two aspects might be emphasized differently by different experimental probes in the normal state, which has led to the two extremes of ideas for the pseudogap, in particular, whether it has a direct relationship with pairing. Our results suggest a plausible reconciliation between them.

Acknowledgments

The authors would like to acknowledge helpful discussions with H. Yao, W.-S. Lee, E. Berg, T. P. Devereaux, S. A. Kivelson, X. J. Zhou, T. Xiang and revision of the

manuscript by R. G. Moore. R.-H.H. thanks G. Yu for kind assistance in the sample preparation and the SGF for financial supports. The work at the ALS is supported by the DOE Office of Basic Energy Science under Contract No. DE-AC02-05CH11231. This work at Stanford is supported by the DOE Office of Science, Division of Materials Science and Engineering, under Contract No. DE-FG03-01ER45929-A001 and a NSF grant DMR-0604701.

I. AUTHOR CONTRIBUTIONS

TS, MF and KY, TA and YK provided and prepared the LSCO $x = 0.11$, LBCO-1/8 and LBCO $x = 0.083$ samples, respectively. SKM, KT and NM maintained the experimental endstation and ensured its high performance. RHH and KT carried out the experiment with the assistance of SKM, NM and TS. RHH did and KT repeated the data analysis and simulations. RHH wrote the paper with helpful suggestions and comments by SKM. ZH and ZXS are responsible for project direction, planning and infrastructure.

II. AUTHOR INFORMATION

Reprints and permission information is available online at http://npg.nature.com/reprintsandpermissions/. The authors declare no competing financial interests. Correspondence and requests for materials should be addressed to Z.-X. Shen (zxshen@stanford.edu).

Supplementary Informatin accompanies this paper on www.nature.com/naturephysics.

---

[1] Timusk, T. & Statt, B. The pseudogap in high-temperature superconductors: an experimental survey. *Rep. Prog. Phys.* **62,** 61-122 (1999) and references therein.

[2] Emery, V. J. & Kivelson, S. A. Superconductivity in bad metals. *Phys. Rev. Lett.* **74,** 3253-3256 (1995).

[3] Honerkamp, C. & Lee, P. A. Staggered flux vortices and the superconducting transition in the layered cuprates. *Phys. Rev. Lett.* **92,** 177002 (2004).

[4] Chakravarty, S., Laughlin, R. B., Morr, D. K. & Nayak, C. Hidden order in the cuprates. *Phys. Rev. B* **63,** 094503 (2001).

[5] Varma, C. M. Non-Fermi-liquid states and pairing instability of a general model of copper oxide metals. *Phys. Rev. B* **55,** 14554-14580 (1997).

[6] Benfatto, L., Caprara, S. & DiCastro, C. Gap and pseudogap evolution within the charge-ordering scenario for superconducting cuprates. *Eur. Phys. J. B* **17,** 95-102 (2000).

[7] Li, J.-X., Wu, C.-Q. & Lee, D.-H. Checkerboard charge density wave and pseudogap of high-T_c cuprate. *Phys. Rev. B* **74,** 184515 (2006)

[8] Das, T., Markiewicz, R. S. & Bansil, A. Competing order scenario of two-gap behavior in hole-doped cuprates. *Phys. Rev. B* **77,** 134516 (2008)

[9] Cataudella, V., De Filippis, G., Mishchenko, A. S., & Nagaosa, N. Temperature dependence of the angle resolved photoemission spectra in the undoped cuprates: Self-consistent approach to the t-J Holstein model. *Phys. Rev. Lett.* **99,** 226402 (2007).

[10] Tanaka, K. *et al.* Distinct Fermi-momentum-dependent energy gaps in deeply underdoped Bi2212. *Science* **314,** 1910-1913 (2006).

[11] Lee, W.-S. *et al.* Abrupt onset of second energy gap at superconducting transition of underdoped Bi2212. *Nature* **450,** 81-84 (2007).

[12] Kondo, T. *et al.* Evidence for two energy scales in the superconducting state of optimally doped $(Bi,Pb)_2(Sr,La)_2CuO_{6+\delta}$. *Phys. Rev. Lett.* **98,** 267004 (2007).

[13] Terashima, K. *et al.* Anomalous momentum dependence of the superconducting coherence peak and its relation to the pseudogap of $La_{1.85}Sr_{0.15}CuO_4$. *Phys. Rev. Lett.* **99,** 017003 (2007).

[14] Boyer, M. C. *et al.* Imaging the two gaps of the high-temperature superconductor $Bi_2Sr_2CuO_{6+x}$. *Nature Phys.* **3,** 802-806 (2007).

[15] Kanigel, A. *et al.* Evolution of the pseudogap from Fermi arcs to the nodal liquid. *Nature Phys.* **2,** 447-451 (2006).

[16] Valla, T., Fedorov, A. V., Lee, J., Davis, J. C. & Gu, G. D. The ground state of the pseudogap in cuprate superconductors. *Science* **314,** 1914-1916 (2006).

[17] Tsuei, C. C. & Kirtley, J. R. Pairing symmetry in cuprate superconductors. *Rev. Mod. Phys.* **72,** 969-1016 (2000).

[18] Tranquada, J. M. *et al.* Quantum magnetic excitations from stripes in copper oxide

superconductors. *Nature* **429,** 534-538 (2004).

[19] Fujita, M., Goka, H., Yamada, K., Tranquada, J. M. & Regnault, L. P. Stripe order, depinning, and fluctuations in $La_{1.875}Ba_{0.125}CuO_4$ and $La_{1.875}Ba_{0.075}Sr_{0.050}CuO_4$. *Phys. Rev. B* **70,** 104517 (2004).

[20] Abbamonte, P. *et al.* Spatially modulated 'Mottness' in $La_{2-x}Ba_xCuO_4$, *Nature Phys.* **1,** 155-158 (2005).

[21] Damascelli, A., Hussain, Z. & Shen, Z.-X. Angle-resolved photoemission of cuprate superconductors. *Rev. Mod. Phys.* **75,** 473-541 (2003) and references therein.

[22] Berg, E., Chen, C.-C. & Kivelson, S. A. Stability of nodal quasiparticles in superconductors with coexisting orders. *Phys. Rev. Lett.* **100,** 027003 (2008).

[23] Mesot J. *et al.* Superconducting gap anisotropy and quasiparticle interactions: a doping dependent photoemission study. *Phys. Rev. Lett.* **83,** 840-843 (1999).

[24] Kordyuk, A. A., Borisenko, S. V., Knupfer, M. & Fink, J. Measuring the gap in angle-resolved photoemission experiments on cuprates. *Phys. Rev. B* **67,** 064504 (2003).

[25] Norman, M. R., Randeria, M., Ding, H. & Campuzano, J. C. Phenomenology of the low-energy spectral function in high-T_c superconductors. *Phys. Rev. B* **57,** R11093-R11096 (1998).

[26] Li, Q., Hücker, M., Gu, G. D., Tsvelik, A. M. & Tranquada, J. M. Two-dimensional superconducting fluctuations in stripe-ordered $La_{1.875}Ba_{0.125}CuO_4$. *Phys. Rev. Lett.* **99,** 067001 (2007).

[27] Berg, E. *et al.* Dynamical layer decoupling in a stripe-ordered high-T_c superconductor, *Phys. Rev. Lett.* **99,** 127003 (2007).

[28] Himeda, A., Kato, T. & Ogata, M. Stripe states with spatially oscillating d-Wave superconductivity in the two-dimensional t-t'-J model. *Phys. Rev. Lett.* **88,** 117001 (2002).

[29] Sasagawa, T. *et al.* Magnetization and resistivity measurements of the first-order vortex phase transition in $(La_{1-x}Sr_x)_2CuO_4$. *Phys. Rev. B* **61,** 1610-1617 (2000).

[30] Adachi, T. *et al.* Magnetic-field effects on the in-plane electrical resistivity in single-crystal $La_{2-x}Ba_xCuO_4$ and $La_{1.6-x}Nd_{0.4}Sr_xCuO_4$ around $x = 1/8$: Implication for the field-induced stripe order. *Phys. Rev. B* **71,** 104516 (2005).

Figure 1: **ARPES spectra and the Fermi surface (FS) of LBCO-1/8.** All data were taken on Sample A with $h\nu$=55 eV at T=21± 2 K (see Supplementary Fig. S1 for data on Sample B with $h\nu$=110 eV). **a**, A coarse FS map having a large momentum coverage. **b**, A fine FS map taken within 2 ∼ 5 hrs after sample cleaving, covering the yellow-shaded region mostly in the second BZ for the detailed spectral analysis. Cuts were taken parallel to the zone diagonal (red arrow) with the polarization of light fixed in plane and orthogonal to the zone diagonal (blue arrow). Each dot of the dotted lines corresponds to an actual sampling momentum position by that cut. The red curves in **a** and blue curves in **b** represent the same tight-binding FS resulting from a global fit to the data (Supplementary Fig. S2). **c**, The momentum distribution curves (MDC's) at E_F, m1 ∼ m10, from cuts #1 ∼ #10 from the nodal to the antinodal as shown in **b**. k_F's determined are indicated by red dots (Supplementary Section IIA & Fig. S9). Note that k_F on cut #10 is already past the zone boundary. The parallel momentum coverage of each MDC does not correspond to the length of that cut shown in **b**. The additional peak features in m9 & m10 are due to the FS crossings in the adjacent quadrant of the BZ as shown in **a**. **d**, The EDC's at k_F, e1 ∼ e10, from cuts #1 ∼ #10, respectively. Red, blue and green arrows indicate the peak intensity, background and peak linewidth in e1, respectively. All spectra are offset vertically for clarity. Labels e1, e4, e7 & e9 in **b** denote the momentum positions of the corresponding EDC's. See Supplementary Section I for additional information.

Figure 2: **The pseudogap function of LBCO-1/8 by the LEG analysis.** **a**, Selected EDC's at k_F, e1, e3, e5, e7 & e8, reproduced from Fig. 1d in an expanded energy scale which are normalized in intensity at the leading edge midpoint (LEM)(Supplementary Fig. S3 & S4). Inset: e1 $\sim$ e4 similarly normalized and shown in a more expanded energy scale to visualize the LEG opening near the node. **b**, LEG plotted as a function of $[cos(k_x) - cos(k_y)]/2$, for LBCO-1/8 Sample A measured at different times after sample cleaving with hν=55 eV; for Sample B measured in different BZ's with hν=55 or 110 eV. T=21$\pm$ 2 K. The results regarding the LEG function at T$\sim$ 20 K were repeated on Sample C (Fig. 4b) and another 6 samples from different batches of growth (not shown). Labels e1, e4, e7 & e9 denote the momentum positions of the corresponding EDC's in Fig. 1d. The black line is a guide to the eye for the ground-state pseudogap function. The LEG values for cuts at different momentum positions for each sample are referenced to the value from the nodal reference cut taken right after that cut. Error bars are determined by the uncertainty of E_F, k_F and the energy window dependence of the LEG by the LEG analysis (see Supplementary Section IIB).

Figure 3: **The nodal gap analysis by curve fitting.** **a**, The E_F-symmetrized EDC's near the node, e1 $\sim$ e4, and fit curves by Fit Model. The arrows are very rough guides to the eye for the centroid of possible peak features in the EDC's. **b**, Δ from different fits without/with different methods of background subtraction (Supplementary Section IIC). Labels e1$\sim$e4 denote the momentum positions of the corresponding EDC's in **a**. The dashed lines are guides to the eye showing the gap slopes by fitting using the two models, respectively. Error bars are determined by the uncertainty of E_F, k_F and the statistical errors of Δ from the fits (with its fitting energy window dependence) but do not include the dependence of background subtraction (see Supplementary Section IIB). A resolution Gaussian with ΔE = 18 meV is used for the convolution with the spectral function for the fitting.

Figure 4: **The doping and temperature dependence of the LEG function. a**, Comparison of the LEG function between LBCO-1/8 (Sample A, within 2 $\sim$ 5 hrs after sample cleaving, reproduced from Fig. 2b), LSCO $x = 0.11$ at T=21$\pm$ 2 K and LBCO $x = 0.083$ at T=19$\pm$ 2 K. The dashed line is an eye guide for the antinodal gap component of LBCO $x = 0.083$. Inset: Comparison between LBCO-1/8 and LBCO $x = 0.083$ of the near-E_F portion of antinodal EDC's taken at the momentum position roughly indicated by the arrow in **a**, showing the absence of the reported anomaly at x$\sim$1/8 in the antinodal pseudogap size [16]. EDC's are normalized in intensity at the LEM and shifted in energy w.r.t. the nodal LEM of each sample. **b**, The LEG function of LBCO-1/8 (Sample C) at T=19$\pm$ 2 K is compared with the one at T=61$\pm$ 2 K. The dashed green curve is a guide to the eye for the 61 K data. Note that the rapid smearing of the distinction between the two gaps as temperature increases is not captured by the extrapolation scheme used in Ref. [15] to obtain the ground-state information based on results at high temperatures. Inset: Detailed temperature dependence in the nodal gap region of Sample A at three selected momentum positions, C1$\sim$C3, as indicated by arrows. Note that C3 is close to the cross-over position of the two gap components. Solid and dashed lines are guides to the eye. See Supplementary Section IIIA for discussion. The same guidelines in black in **a** & **b** for LBCO-1/8 at low temperature are reproduced from Fig. 2b. All data were taken with hν=55 eV. The same nodal referencing scheme is used for the LEG values as in Fig. 2b. Error bars are determined by the uncertainty of E_F, k_F and the energy window dependence of the LEG by the LEG analysis (see Supplementary Section IIB).

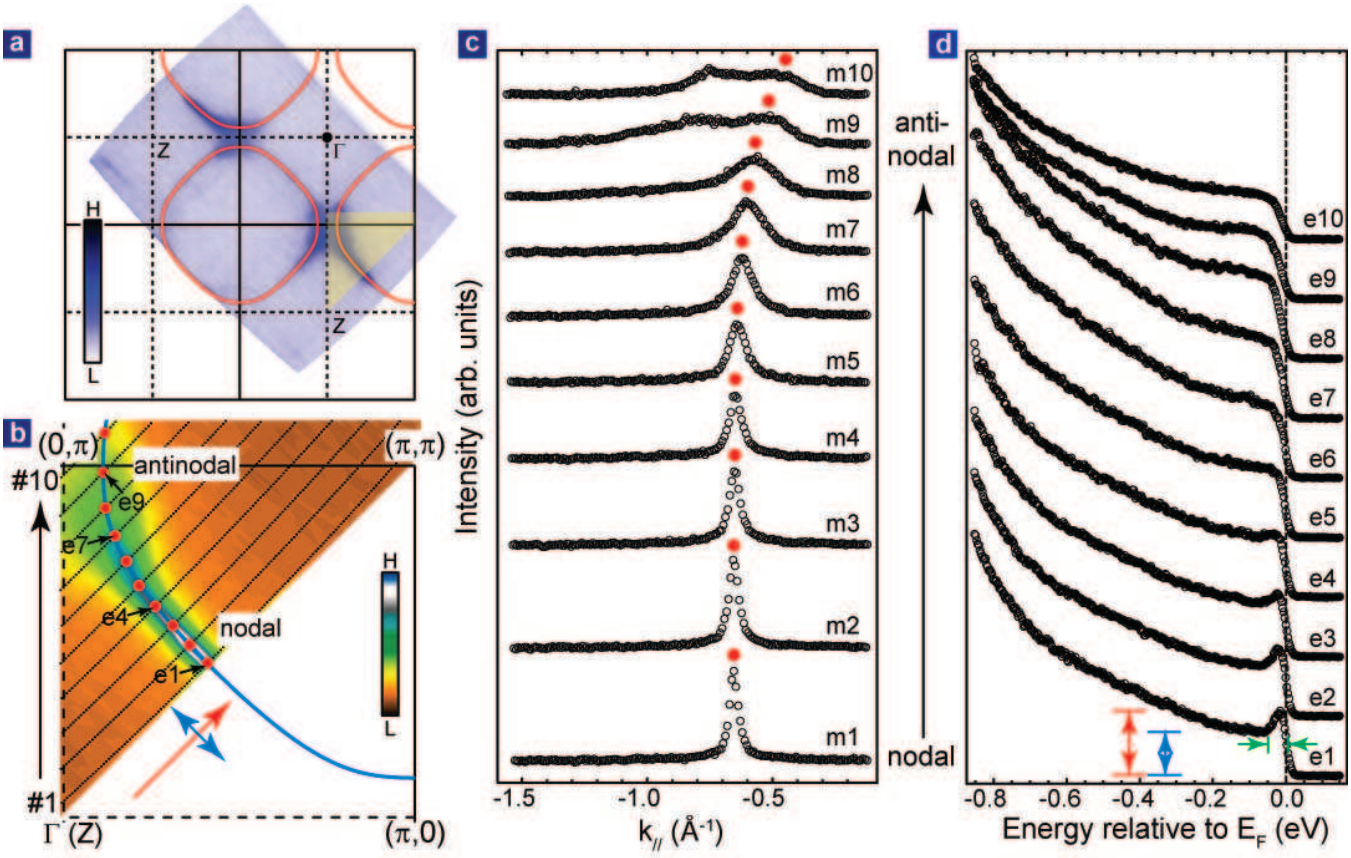
a
Z
Γ
H
L
Z
b
(0,π)
(π,π)
#10
antinodal
e9
e7
e4
nodal
e1
H
L
#1
Γ (Z)
(π,0)
c
m10
m9
m8
m7
m6
m5
m4
m3
m2
m1
Intensity (arb. units)
-1.5
-1.0
-0.5
k// (Å-1)
d
anti-
nodal
nodal
e10
e9
e8
e7
e6
e5
e4
e3
e2
e1
-0.8
-0.6
-0.4
-0.2
0.0
Energy relative to EF (eV)

Figure 1

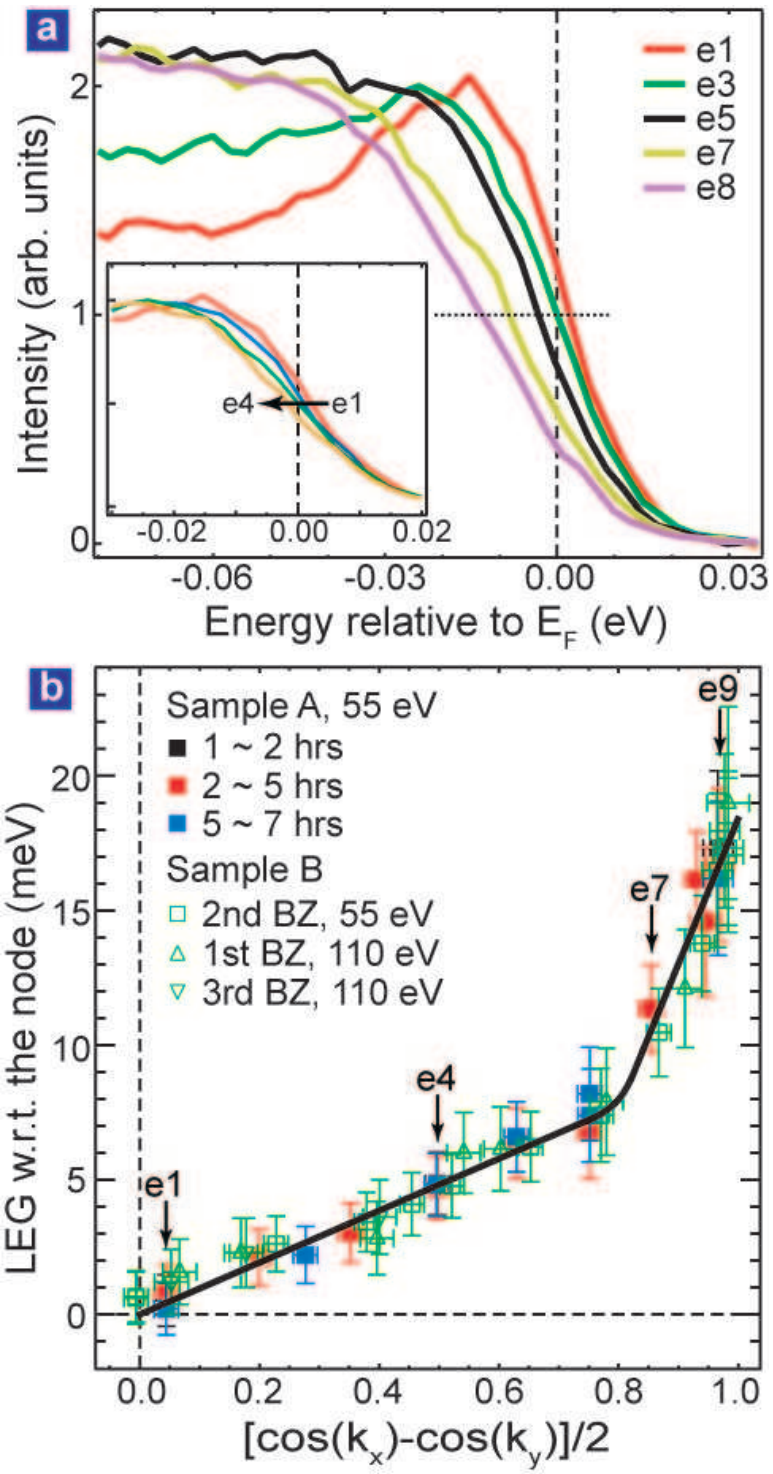
a
e1
e3
e5
e7
e8
Intensity (arb. units)
2
1
0
e4
e1
-0.02
0.00
0.02
-0.06
-0.03
0.00
0.03
Energy relative to E_F (eV)
b
Sample A, 55 eV
1 ~ 2 hrs
2 ~ 5 hrs
5 ~ 7 hrs
Sample B
2nd BZ, 55 eV
1st BZ, 110 eV
3rd BZ, 110 eV
e9
e7
e4
e1
LEG w.r.t. the node (meV)
20
15
10
5
0
0.0
0.2
0.4
0.6
0.8
1.0
[cos(k_x)-cos(k_y)]/2

Figure 2

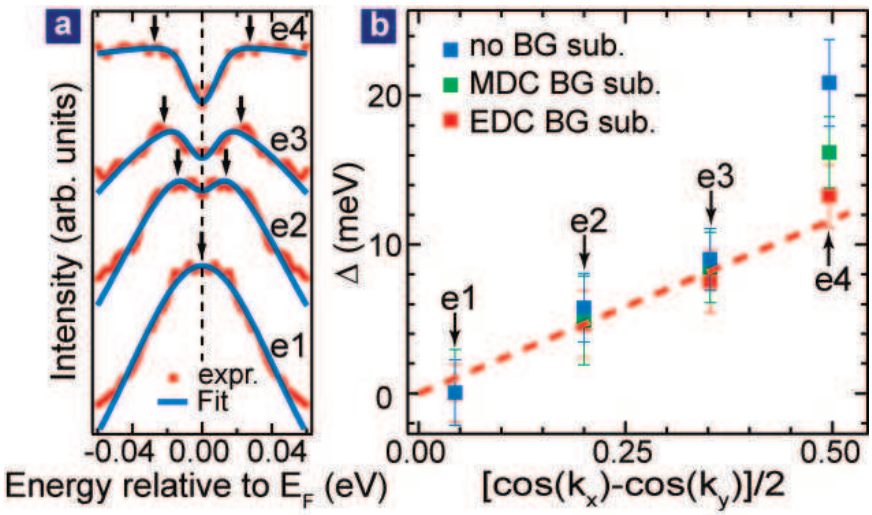
a
e4
e3
e2
e1
Intensity (arb. units)
expr.
Fit
-0.04 0.00 0.04
Energy relative to E_F (eV)
b
no BG sub.
MDC BG sub.
EDC BG sub.
20
10
0
Δ (meV)
e1
e2
e3
e4
0.00
0.25
0.50
[cos(k_x)-cos(k_y)]/2

Figure 3

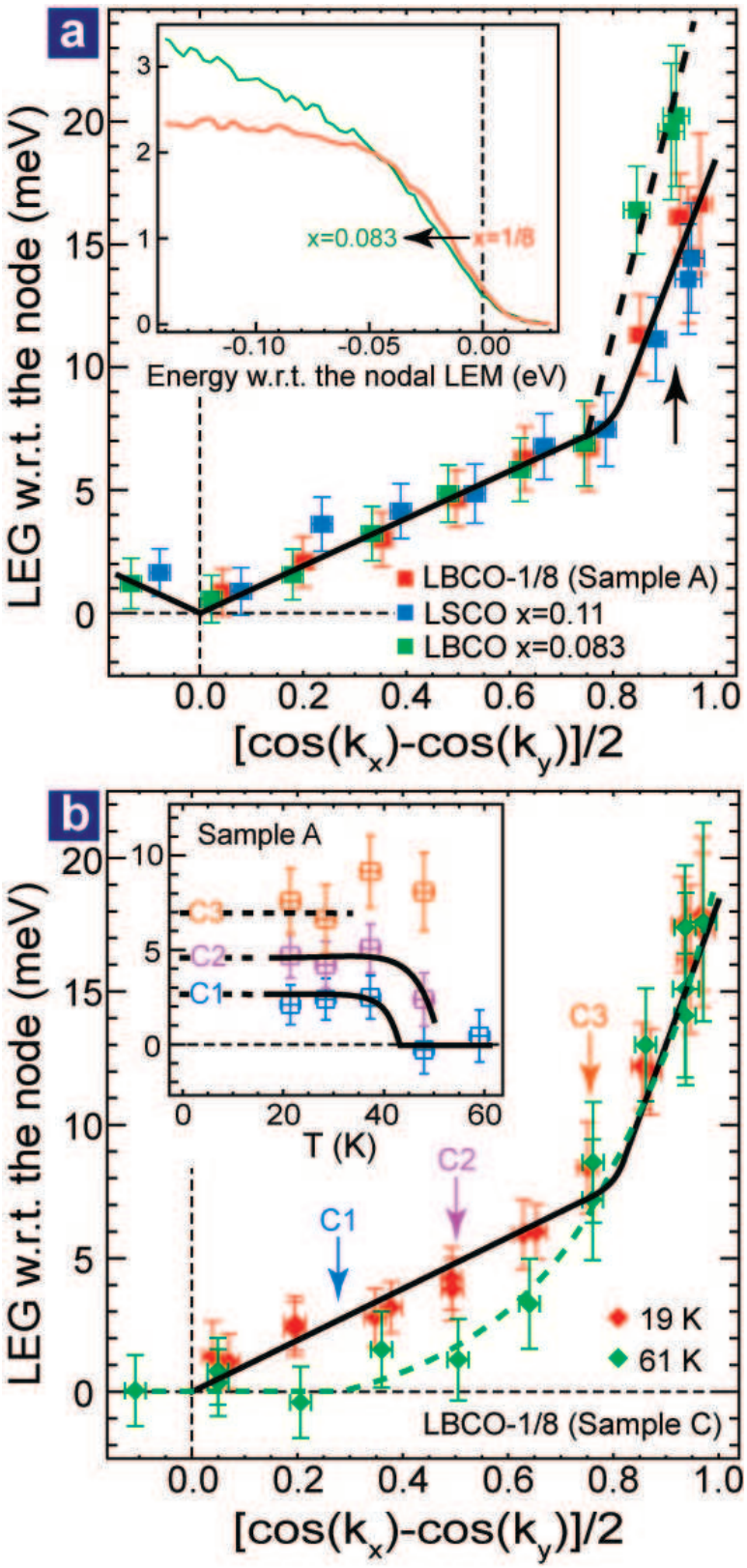
a
LEG w.r.t. the node (meV)
[cos(k_x)-cos(k_y)]/2
x=0.083
x=1/8
Energy w.r.t. the nodal LEM (eV)
LBCO-1/8 (Sample A)
LSCO x=0.11
LBCO x=0.083
b
Sample A
C1
C2
C3
T (K)
19 K
61 K
LBCO-1/8 (Sample C)

Figure 4